Theory of Raman spectra of heavily doped semiconductor multiple quantum wells

Yia-Chung Chang
Department of Physics and Materials Research Laboratory, University of Illinois at Urbana-Champaign, 1110 West Green Street, Urbana, Illinois 61801-3080

Huade Yao
Center for Microelectronic and Optical Materials Research, and Department of Electrical Engineering, University of Nebraska, Lincoln, Nebraska 68588-0511

(Received 8 March 1996; revised manuscript received 31 May 1996)

We present theoretical studies of the Raman spectra of heavily doped GaAs-$Al_xGa_{1-x}As$ multiple quantum wells in an attempt to understand the effects of heavy two-dimensional (2D) doping on the electronic structures and optical properties of semiconductors. Samples of GaAs-$Al_xGa_{1-x}As$ multiple quantum wells with $x=0.2$ and 0.4, well-barrier widths around 100 Å, and 2D electron densities up to more than 1×10^{13} cm^{-2} are examined. Intersubband and intrasubband Raman plasmon modes are calculated with an energy-dependent effective-mass theory, which takes into account the band nonparabolicity. The screened external potential due to impurity and electron charge distribution including the exchange and correlation effects are calculated self-consistently within the local-density approximation. The resulting Raman spectra are found to be sensitive to the shape of the screened potential, and they are in qualitative agreement with experimental data. [S0163-1829(96)01039-9]

I. INTRODUCTION

Doping of semiconductor quantum wells has been of interest to electronic device industries and scientific research societies. Electrons doped in narrow quantum wells (well widths $\leqslant 100$ Å) form a two-dimensional electron gas (2DEG), and populate in confined quantum states in the wells. There have been many investigations over the years of properties of 2DEG related with doped quantum wells or δ-doped semiconductors.[1–7] The fundamental electronic excitations of doped semiconductor quantum wells are single-particle excitations and the collective modes which include both intrasubband and intersubband plasmons. These collective modes can interact with longitudinal-optical phonons and single-particle excitations (leading to Landau damping of the plasmon) when their energies nearly coincide. A general review of the properties of collective modes and their interaction with phonons in semiconductor quantum wells can be found in Ref. 8.

Raman spectroscopy is the ideal tool to probe the collective electronic excitations in semiconductors, and it has been used with great success to study heavily doped semiconductors.[9,10] The results can be fully understood in terms of the phonon-plasmon coupled modes within the content of linear-response theory. The situation in quantum wells is more complicated due to the existence of many subbands. Depending on the polarizations of the incident and scattered light in the measurement, the Raman scattering can probe either the charge-density excitation (CDE) when both polarizations are parallel, or the spin-density excitation (SDE) when the two polarizations are perpendicular.[1] The difference between CDE and SDE energies in the Raman spectra is called the ''depolarization shift.'' Theoretical calculations of Raman spectra of low-doping quantum wells without including the self-consistent potential have been reported.[3,11,12] However, systematic theoretical studies of the optical properties of heavily doped quantum wells have not been fully conducted. The main differences between the low-doping and high-doping case are as follows: (1) carrier energies of interest are high, so the nonparabolicity effect can not be ignored; (2) the band bending due to the self-consistent potential and exchange-correlation effects becomes important; and (3) higher subbands and many unconfined (above-barrier) states are needed to describe the intersubband transitions correctly.

In this paper, we report theoretical studies of the Raman spectra of heavily doped GaAs-$Al_xGa_{1-x}As$ multiple quantum wells in an attempt to understand 2D doping on the electronic structures and optical properties in semiconductors. Cases of well-doped and barrier-doped multiple quantum wells are studied. Samples of GaAs-$Al_xGa_{1-x}As$ multiple quantum wells with $x=0.2$ and 0.4, well-barrier widths around 100 Å, and 2D electron densities up to more than 1×10^{13} cm^{-2} are examined. Intersubband and intrasubband Raman plasmon modes for realistic samples which involve eight quantum wells are theoretically analyzed. The number of quantum wells is chosen so that the total length of multiple quantum wells is comparable to the penetration depth of the incident photon in order to maximize the signal-to-noise ratio in the Raman measurements. In our calculations, the energy-band nonparabolicity, the many-body-exchange correlation, and the dynamic dielectric screening are all taken into account. To simplify the computation, an ''effective Hamiltonian'' method is developed, which is shown to improve substantially the efficiency of the calculation of Raman spectra compared with the direct evaluation of the density-density correlation function. The resulting Raman spectra are found to be sensitive to the shape of the screened potential, which in turn depends strongly on the doping profile. A comparison between theory and experiment for the

well-doped case is presented. More detailed experimental studies of both the well- and barrier-doped cases will be presented elsewhere.[13]

II. THEORY

We shall consider Raman spectra due to charge-density excitations of a heavily doped GaAs-$Ga_{1-x}Al_xAs$ multiple-quantum-well system. The electronic states of the multiple quantum well are described in an energy- and position-dependent effective-mass approximation, which takes into account both the nonparabolicity effect and the difference in effective mass for the well and barrier materials. In this model, the energy of an electron in a quantum well is described by

$$E(\mathbf{k})=\frac{k^2}{1+[E(\mathbf{k})+\eta V(z)]/E_g}, \tag{1}$$

where E_g is the fundamental gap of GaAs, $E(\mathbf{k})$ is the energy of the electron in the system measured with respect to the bottom of the well, and $V(z)$ is the quantum-well potential which is zero for z in the well and V_0 in the barrier. η is an empirical factor less than 1, which is to be determined. Here and henceforth we use the units in which the energy is measured in the effective rydbergs, $\mathrm{Ry}^*\equiv 13.6$ eV $m_0/m^*(0)$, where $m^*(0)$ is the effective mass of the well material, and the distance measured in bohr ($a_B=0.529$ Å). For an electron in the well, $V(z)=0$, and the above relation is the same as that given by Bastard's two-band $\mathbf{k}\cdot\mathbf{p}$ model,[14] i.e.,

$$E(1+E/E_g)=k^2. \tag{2}$$

Thus the band nonparabolicity is properly taken into account. For an electron in the barrier material [with $V(z)$ equal to the band offset V_0], Eq. (1) leads to a nonparabolic effective mass expression with the zone-center effective mass $(\partial E/[\partial(k^2)])|^{-1}_{E=V_0}=m^*(0)[1+(2+\eta)V_0/E_g]$, which is larger than the effective mass of the well material. Here we have used $E=V_0$, the minimum energy of the electron in the barrier material. We now determine the empirical factor η. For GaAs, $m^*(0)=0.065m_0$ (m_0 is the free-electron mass) at $T=300$ K, including the polaron effect.[15] The band gap for $Al_xGa_{1-x}As$ at room temperature is given by[16]

$$E_g(x)=(1.424+1.247x)\ \text{eV},$$

and the quantum-well depth is given by

$$V_0(x)=[E_g(x)-E_g(0)]0.65,$$

where the 65/35% rule has been used.[17] Using the energy-dependent effective-mass relation, we obtain an effective mass of $Al_xGa_{1-x}As$ to be $0.065[1+0.569(2+\eta)x]m_0$. Comparing this expression with the experimental value[18] of $0.065(1+1.239x)m_0$, we obtain $\eta\approx 0.18$. So Eq. (1) is suitable for describing electrons in $Al_xGa_{1-x}As$/GaAs quantum wells even when the electron energy is higher than the barrier height. This is what we need for studying collective modes of doped $Al_xGa_{1-x}As$/GaAs quantum wells involving unconfined states.

For practical purposes, it is rather inconvenient to use expression (1) for calculating electronic states of a quantum well, since it is difficult to handle the kinetic-energy operator corresponding to [with $k_z=-i(\partial/\partial z)$]

$$E(k_z)=\frac{E_g+\eta V(z)}{2}\left[\left(1+\frac{4E_gk_z^2}{[E_g+\eta V(z)]^2}\right)^{1/2}-1\right], \tag{3}$$

which is the solution to Eq. (1) with $k_\parallel=0$. However, if both k_z^2 and ηV_0 are much less than E_g, we can approximate the above expression by (keeping only the first order term of $\eta V/E_g$)

$$E(k_z)=\frac{E_g}{2}\left[\left(1+\frac{4k_z^2}{E_g}\right)^{1/2}-1\right]-k_z^2\eta V(z)/E_g. \tag{4}$$

Note that the last term (referred to as T_1) is not Hermitian if we let $k_z=-i(\partial/\partial z)$. To circumvent this difficulty, we replace the term by $T_1=\overleftarrow{\partial}_z(\eta V(z)/E_g)\overrightarrow{\partial}_z$, where $\overleftarrow{\partial}$ means ''taking the derivative of a function to the left,'' and $\overrightarrow{\partial}$ means ''taking the derivative of a function to the right.'' The above procedure is valid, since the expectation value of T_1 in a state completely confined in a given material (well or barrier) gives the right correction to its kinetic energy. We can now solve the quantum well problem using a plane-wave basis.

For ease in computation, we consider a multiple quantum well with well width L_w, barrier width L_b, and depth V_0 placed inside a large square well of width L ($L>>L_w+L_b$) and with an infinite potential barrier (see Fig. 1). The width L can be arbitrarily increased until the final results are insensitive to L, at which point the results are correct for an isolated multiple-quantum-well system. Let T_n and $\phi_n(z)$ be the kinetic energies and eigenfunctions of an electron in the infinite well with $V_0=0$ and $k_\parallel=0$, viz.,

$$T_n=\frac{E_g}{2}\left[\left(1+\frac{4k_n^2}{E_g}\right)^{1/2}-1\right], \tag{5}$$

with $k_n=n\pi/L$ and

$$\phi_n(z)=\left(\frac{2}{L}\right)^{1/2}\sin(n\pi z/L). \tag{6}$$

The eigenstates of the entire system with the multiple quantum wells present and including the effects due to the mismatch of effective masses inside and outside the quantum wells are expanded in terms of the basis functions ϕ_n as

$$\xi_i(z)=\sum_{n=1}^{N}C_n^i\phi_n(z). \tag{7}$$

The expansion coefficients C_n are obtained by solving the Schrödinger equation for the system self-consistently within the basis set (including the correction due to T_1), i.e.,

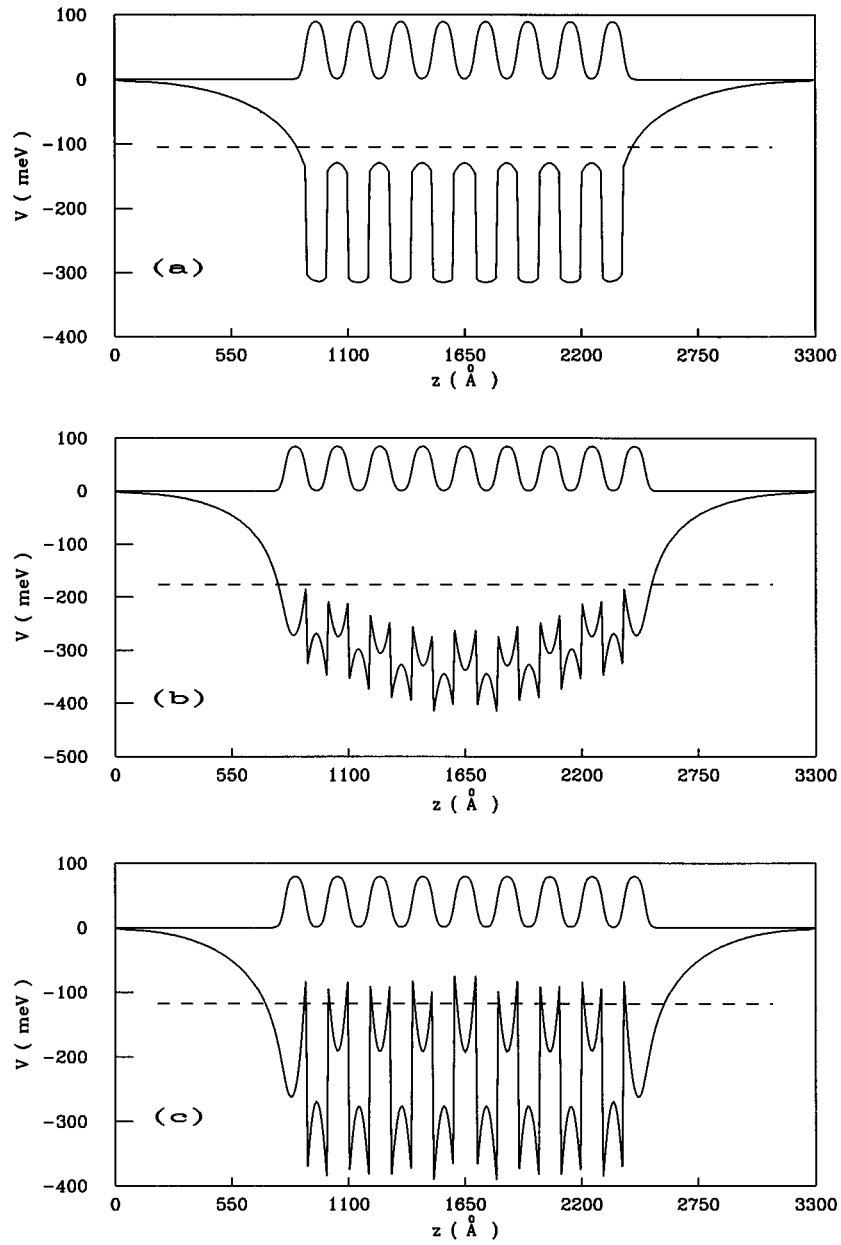

FIG. 1. Total potential seen by an electron (lower curve) in a multiple GaAs-$Al_xGa_{1-x}As$ quantum well with (a) $x=0.2$, doped in the well, and $n_{2D}\approx 1.06\times 10^{13}$ cm^{-2}, (b) $x=0.2$, doped in the barrier, and $n_{2D}\approx 1.2\times 10^{13}$ cm^{-2}, and (c) $x=0.4$, doped in the barrier, and $n_{2D}\approx 1.36\times 10^{13}$ cm^{-2}. The upper curve shows the doping profile. The dashed line indicates the Fermi level.

$$\sum_{n'} (T_n\delta_{n,n'}+\langle n|T_1|n'\rangle+\langle n|V_{mqw}|n'\rangle + \langle n|V_{\rm sc}|n'\rangle)C^i_{n'}=E^0_iC^i_n, \tag{8}$$

where V_{mqw} denotes the multiple-quantum-well potential of interest, and $V_{\rm sc}$ is the screened potential due to impurities and free carriers. A total of 200 basis functions will be used in our calculations. We assume that the impurity charge distribution is uniform in the x-y plane and is described by a z-dependent function $\rho_I(z)$. For uniform doping within a quantum well of width L_w, we assume

$$\rho_I(z)=\frac{en_{2D}}{L_w}g(z),$$

where e denotes the electron charge, n_{2D} is the average layer doping density, which equals the average 2D carrier density, and $g(z)$ is a hatlike function defined as

$$g(z)=(e^{(|z|-L_w/2)/b}-1)^{-1}\Big/\int(e^{(|z|-L_w/2)/b}-1)^{-1}dz. \tag{9}$$

The parameter b describes the spread of the impurity concentration around the interface. Throughout this paper, we shall assume $b=10$ Å. Similarly for uniform doping within a quantum barrier, we replace L_w by L_b in the above equation. The carrier charge distribution is denoted $\rho_e(z)$, which can be calculated once the subband energies $E_i(\mathbf{k}_\parallel)$ and eigenfunctions $\xi_i(z)$ are found. We have

$$\rho_e(z)=-\frac{2e}{A}\sum_i\sum_{\mathbf{k}_\parallel} f[\mu-E_i(\mathbf{k}_\parallel)]|\xi_i(z)|^2 \equiv -e\sum_i n_i^{2D}|\xi_i(z)|^2, \tag{10}$$

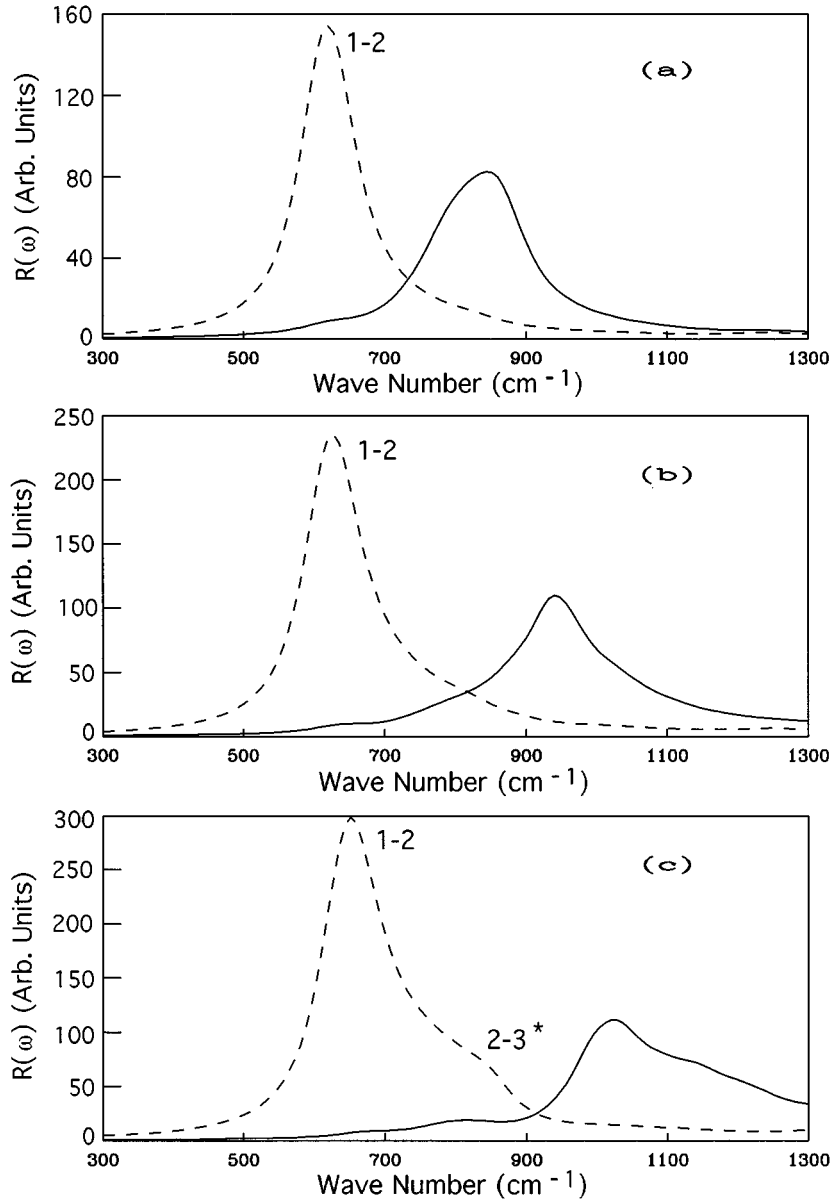

FIG. 2. Raman spectra of well-doped multiple GaAs-$Al_{0.2}Ga_{0.8}As$ quantum wells with (a) $n_{2D}=3.0\times10^{12}$ cm^{-2}, (b) $n_{2D}=5.7\times10^{12}$ cm^{-2}, and (c) $n_{2D}=1.06\times10^{13}$ cm^{-2} per quantum well. $L_w=L_b=100$ Å. Dashed curves: without Coulomb interaction. Solid curves: full calculation.

where $n_i^{2D}=\Sigma_{\mathbf{k}_\parallel} f[\mu-E_i(\mathbf{k}_\parallel)]$ denotes the 2D carrier density for subband i, μ is the chemical potential, and $f(\mu-E)=1/(e^{(E-\mu)/k_BT}+1)$ is the Fermi distribution function. The subband energy $E_i(\mathbf{k}_\parallel)$ is derived as follows. From Eq. (1), by taking the derivative of $E(\mathbf{k})$ with respect to $k_\parallel^2$ we can express the kinetic energy at finite $\mathbf{k}$ as the kinetic energy at $k_\parallel=0$ plus a quadratic term in $k_\parallel$ (ignoring higher-order terms). We have

$$E(\mathbf{k})\approx E(k_\parallel=0)+\frac{k_\parallel^2}{1+(2E(\mathbf{k})+\eta V)/E_g}. \tag{11}$$

Replacing the operator V by its expectation value V_i in the state i, $E(\mathbf{k})$ by the subband energy $E_i(\mathbf{k}_\parallel)$, and $E(k_\parallel=0)$ by E_i^0, we obtain

$$E_i(\mathbf{k}_\parallel)\approx\{\sqrt{(E_g+\eta V_i-2E_i^0)^2+8[E_g k_\parallel^2+(E_g+\eta V_i)E_i^0]}-(E_g+\eta V_i-2E_i^0)\}/4. \tag{12}$$

We define $\rho_t(z)=\rho_I(z)+\rho_e(z)$ to be the total charge distribution, which satisfies the charge neutrality condition

$$\int dz\rho_t(z)=0.$$

The self-consistent Hartree potential seen by an electron is given by

$$V_H(z)=-\frac{e}{\epsilon(0)}\int d^3r'\frac{\rho_t(z')}{|\mathbf{r}-\mathbf{r}'|}=2\pi\frac{e}{\epsilon(0)}\int dz'\rho_t(z')|z-z'|, \tag{13}$$

where the charge neutrality condition has been used and $\epsilon(0)$ is the static dielectric constant. In our calculations, we use $\epsilon(0)=13.18-3.12x$, where x is the Al mole fraction in $Al_xGa_{1-x}As$. The net screened potential is the Hartree potential plus the exchange correlation potential, i.e.,

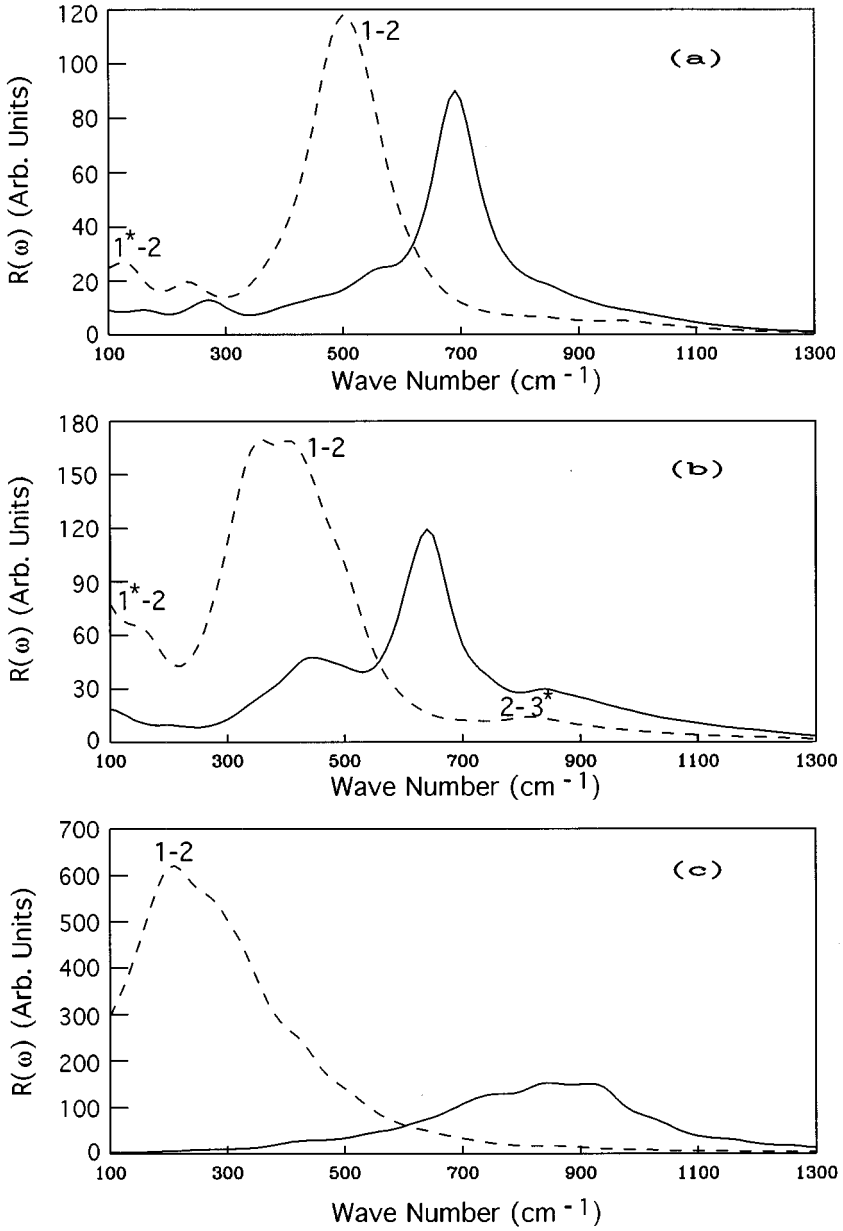

FIG. 3. Raman spectra of barrier-doped multiple GaAs-$Al_{0.2}Ga_{0.8}As$ quantum wells with (a) $n_{2D}=2.9\times10^{12}$ cm^{-2}, (b) $n_{2D}=5.4\times10^{12}$ cm^{-2}, and (c) $n_{2D}=1.20\times10^{13}$ cm^{-2} per quantum well. $L_w=L_b=100$ Å. Dashed curves: without Coulomb interaction. Solid curves: full calculation.

$$V_{sc}(z)=V_H(z)+V_{\rm xc}(z),$$

where $V_{\rm xc}(z)$ denotes the Kohn-Sham exchange correlation potential[19] within the local-density approximation (LDA). $V_{\rm xc}(z)$ is a function of $\rho_e(z)$ with an accurate relation given by Ceperley and Alder[20] for the free-electron gas in a jellium model. A convenient interpolation formula for $V_{\rm xc}(z)$ as a function of ρ_e can be found in Ref. 21.

The Raman intensity due to charge excitation is related to the density-density correlation function $D(z,z',\omega)$ by

$$R(\omega)=-\,\mathrm{Im}\int dz\,dz' e^{-iq_z(z-z')}D(z,z',\omega), \qquad (14)$$

where $D(z,z')$ is expanded in terms of eigenfunctions of the system as

$$D(z,z')=\sum_{i,j,k,l} D_{ij,kl}\xi_i(z)\xi_j(z)\xi_k(z')\xi_l(z'). \qquad (15)$$

In the random-phase approximation (RPA), we have[12]

$$D_{ij,kl}=D^0_{kl}\delta_{ik}\delta_{jl}+\sum_{mn} D^0_{ij}V_{ij,mn}(q)D_{mn,kl}, \qquad (16)$$

where

$$D^0_{ij}=2\sum_{\mathbf{k}}\frac{f[E_j(\mathbf{k}+\mathbf{q})]-f(E_i(\mathbf{k}))}{E_j(\mathbf{k}+\mathbf{q})-E_i(\mathbf{k})-\hbar\omega}$$

with $f(E)$ being the Fermi-Dirac function and

$$V_{ij,mn}(q)=\int dz\,dz'\frac{2\pi e^2}{\epsilon(\infty)q}e^{-q|z-z'|}\times\xi_i(z)\xi_j(z)\xi_m(z')\xi_n(z'), \qquad (17)$$

where $\epsilon(\infty)$ is the high-frequency dielectric constant. In our calculations, we use $\epsilon(\infty)=10.92(1-x)+8.16x$ (Ref. 18). Note that the index ij (kl) labels an excitation in which the

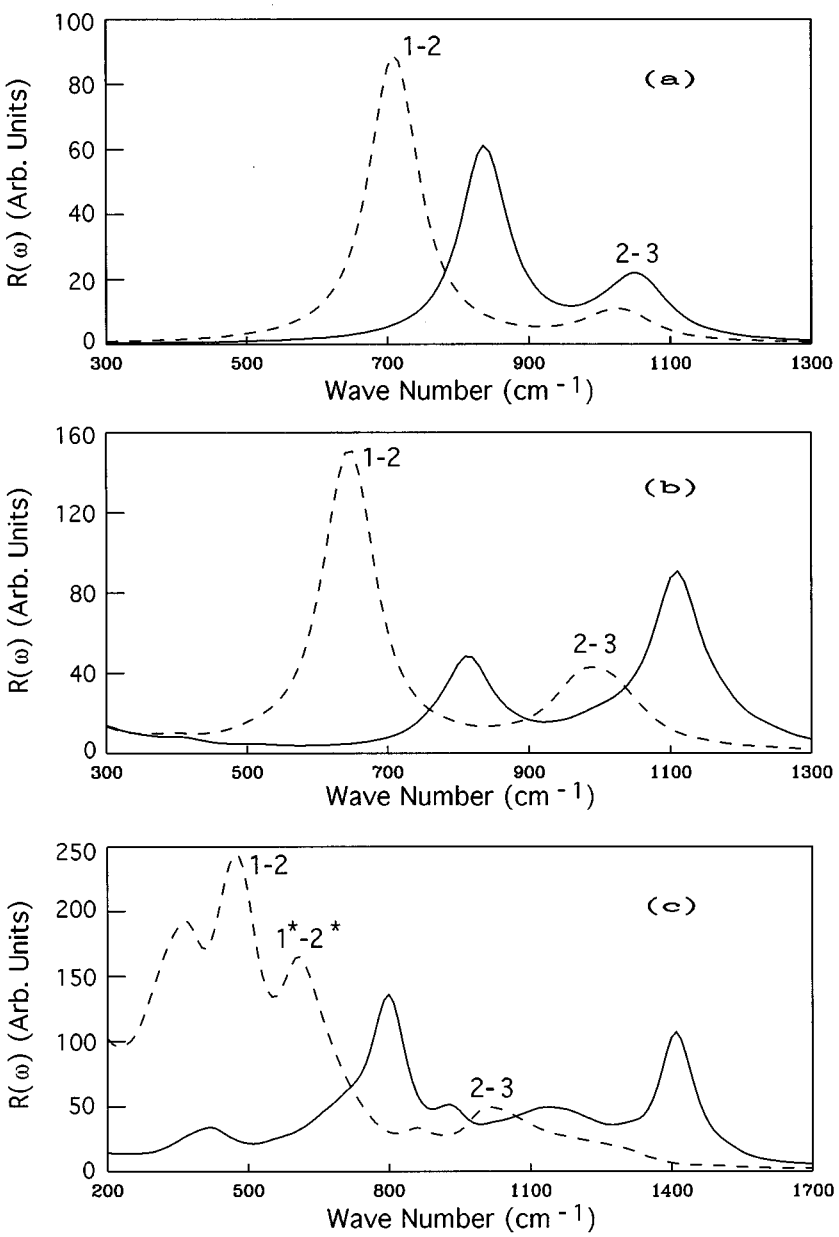

FIG. 4. Raman spectra of barrier-doped multiple GaAs-$Al_{0.4}Ga_{0.6}As$ quantum wells doped with (a) $n_{2D}=1.9\times10^{12}$ cm^{-2}, (b) $n_{2D}=4.4\times10^{12}$ cm^{-2}, and (c) $n_{2D}=1.36\times10^{13}$ cm^{-2} per quantum well. $L_w=L_b=100$ Å. Dashed curves: without Coulomb interaction. Solid curves: full calculation.

electron is excited from state $i(k)$ to $j(l)$. In this paper, we are only concerned with intersubband plasmon transitions with energies much higher than the optical-phonon energy; thus plasmon-phonon coupling has been ignored. Furthermore, since $V_{ij,kl}$ is invariant under the exchange of indices $ij\rightarrow ji$ and $kl\rightarrow lk$, we can add up the $ij(kl)$ and $ji(lk)$ components in Eq. (16) to obtain

$$\overline{D}_{ij,kl}=\overline{D^0_{kl}}\delta_{ik}\delta_{jl}+\sum_{m\leqslant n}\overline{D^0_{ij}}V_{ij,mn}\overline{D}_{mn,kl}, \quad i\leqslant j;k\leqslant l, \tag{18}$$

where $\overline{D}_{ii,kk}\equiv D_{ii,kk}$, $\overline{D^0_{ii}}\equiv D^0_{ii}$ $\overline{D}_{ij,kl}\equiv D_{ij,kl}+D_{ij,lk}+D_{ji,kl}+D_{ji,lk}$ ($i<j$ and $k<l$), and $\overline{D^0_{ij}}\equiv D^0_{ij}+D^0_{ji}$ ($i<j$). Substituting (15) and (18) into (14) yields

$$R(\omega)=-\,\mathrm{Im}\sum_{i\leqslant j,k\leqslant l}\overline{D}_{ij,kl}p^*_{ij}(q_z)p_{kl}(q_z), \tag{19}$$

where $p_{ij}(q_z)\equiv\int dz e^{iq_zz}\xi_i(z)\xi_j(z)$. The matrix elements $V_{ij,mn}(q)$ and $p_{ij}(q_z)$ are given in the Appendix.

The direct evaluation of $R(\omega)$ from Eq. (19) for every frequency is very time consuming. To simplify the problem, we shall develop an ''effective Hamiltonian method'' as described below. We first note that Eq. (16) is just the Dyson's equation, which can be rewritten as

$$\overline{D}^{-1}_{ij,kl}=(\overline{D^0_{ij}})^{-1}\delta_{ik}\delta_{jl}-V_{ij,kl}.$$

For the small values of q considered here,[12]

$$D^0_{ij}\approx\begin{cases}\dfrac{n_i-n_j}{\hbar\omega-E^0_{ij}} & \text{for } i\neq j\\[2ex] \dfrac{n_iq^2}{m^*\omega^2} & \text{for } i=j,\end{cases} \tag{20}$$

and

$$\overline{D_{ij}^0}=\frac{2E_{ij}^0(n_i-n_j)}{(\hbar\omega)^2-(E_{ij}^0)^2} \text{ for } i<j,$$

where n_i denotes the 2D electron density in subband i, and $E_{ij}^0=E_j^0-E_i^0$ is the subband energy difference.

Introduce the scaling factor

$$A_{ij}\equiv\begin{cases}\sqrt{2E_{ij}^0(n_i-n_j)} & \text{for } i<j\\ \sqrt{n_i\hbar^2q^2/m^*} & \text{for } i=j,\end{cases}$$

and letting $\widetilde{D}_{ij,kl}^{-1}\equiv A_{ij}\overline{D}_{ij,kl}^{-1}A_{kl}$, $(\widetilde{D}_{ij}^0)^{-1}\equiv A_{ij}(\overline{D_{ij}^0})^{-1}A_{ij}$, and $\widetilde{V}_{ij,kl}\equiv A_{ij}V_{ij,kl}A_{kl}$, we then have

$$\widetilde{D}^{-1}=(\hbar\omega)^2-\widetilde{H},$$

where

$$\widetilde{H}_{ij,kl}\equiv(E_{ij}^0)^2\delta_{ik}\delta_{jl}+\widetilde{V}_{ij,kl}.$$

$\widetilde{H}$ behaves like an ''effective Hamiltonian,'' with diagonal elements being the square of excitation energies plus the interaction term. Since $\widetilde{H}$ is independent of ω, we only have to find the transformation matrix S which diagonalizes $\widetilde{H}$, and we immediately obtain

$$\widetilde{D}_{ij,kl}=\sum_{mn} S_{ij,mn}[(\hbar\omega)^2-\lambda_{mn}]^{-1}S_{kl,mn},$$

where λ_{mn} denote the mnth eigenvalue of $\widetilde{H}$. Finally, we have

$$R(\omega)=-\operatorname{Im}\sum_{m\leqslant n}[(\hbar\omega+i\Gamma)^2-\lambda_{mn}]^{-1}|\widetilde{p}_{mn}(q_z)|^2, \quad (21)$$

where

$$\widetilde{p}_{mn}(q_z)\equiv\sum_{ij} p_{ij}(q_z)A_{ij}S_{ij,mn}.$$

Note that we have introduced the broadening factor Γ in the last step. The effective Hamiltonian method introduced here not only reduces the computational effort but also makes the results much easier to interpret. Using Eq. (21), we can view the Raman spectrum as a linear superposition of many intersubband plasmon transitions, each having a transition energy $\sqrt{\lambda_{mn}}$ and oscillator strength $|\widetilde{p}_{mn}|^2$. Due to the repulsive interaction $\widetilde{V}$, each transition energy is shifted up from the intersubband energy E_{mn}^0 This shift in energy shall be called the ''Coulomb shift,'' to be distinguished from the depolarization shift.

It is easy to show from Eq. (21) that the following sum rule holds,

$$\int R(\omega)\omega d\omega=\frac{\pi}{2}\sum_{m\leqslant n}|\widetilde{p}_{mn}(q_z)|^2=\frac{\pi}{2}\sum_{m\leqslant n}|A_{mn}p_{mn}(q_z)|^2. \quad (22)$$

So the integrated area of $\omega R(\omega)$ remains unchanged whether we include the Coulomb interaction or not.

For heavily doped quantum wells, many subbands (including unconfined states) are filled with electrons. Thus the number of states (N) to be considered can be quite large, and the dimension of the $\widetilde{H}$ matrix [which goes like $N(N+1)/2$] become too large to be handled efficiently. Let us consider the charge excitations involving only unconfined states, i.e., with subband index $i>N_c$, where N_c is the number of quantum-confined states. If both subbands i and j are unconfined states and their energies are close; then the electron populations are almost the same and we have $A_{ij}\approx 0$ for $i\neq j$. Furthermore if subbands i and j are greatly separated in energy, we have $V_{ij,kl}(q)\approx 0$ due to the quickly oscillating nature of the function $\xi_i(z)\xi_j(z)$. Consequently, we can ignore the matrix elements $\widetilde{H}_{ij,kl}$ when either $i\neq j$ with $i,j>N_c$ or $k\neq l$ with $k,l>N_c$. By keeping only the intersubband excitations involving at least one confined state and the intrasubband excitations for all subbands with $i\leqslant N$, we can reduce the dimension of the $\widetilde{H}$ matrix from $N(N+1)/2$ to $(N_c+1)N-N_c(N_c+1)/2$.

III. RESULTS

All results shown here are obtained from Eq. (21), with the temperature set at 300 K and the broadening parameter Γ set at 5 meV. The momentum transfer parallel to the plane ($q_\parallel$) is assumed to be nearly zero, consistent with the backscattering geometry used in experiment. In Fig. 1, we plot the total potential, $V_{mqw}+V_{\rm sc}$ seen by an electron (lower curve) and the doping profile (upper curve) in a multiple GaAs-$Al_xGa_{1-x}As$ quantum well. We choose $L_w=L_b=100$ Å and $N_w=8$. Both the buffer and cladding layers are undoped $Al_xGa_{1-x}As$, and are assumed to be 800 Å thick. In (a), $x=0.2$, and each quantum well is doped with $n_{2D}=1.06\times10^{13}$ cm^{-2}. In (b), $x=0.2$ and each quantum barrier is doped such that $n_{2D}=1.20\times10^{13}$ cm^{-2}. In (c), $x=0.4$ and each quantum barrier is doped such that $n_{2D}=1.3\times10^{13}$ cm^{-2}. The doping profile is given by Eq. (9) and the impurity distribution is plotted on top of the potential. The energy zero is taken to be the conduction-band minimum of $Al_{0.2}Ga_{0.8}As$ far away from the doped region. The dashed line indicates the Fermi level. Due to heavy doping the potential of the entire multiple-quantum-well (MQW) region is dramatically lowered by the self-consistent screened potential. In the limit of zero width of the MQW region, the system is reduced to a δ-doped $Al_xGa_{1-x}As$ system, and the total potential approaches a V-shaped potential as expected. In each quantum well there are two confined subbands, which are heavily occupied. The charge-density excitation from these occupied levels to the nearly unoccupied excited states near the Fermi level leads to prominent structures in the Raman spectra.

There are three major differences between the well-doped and barrier-doped multiple quantum wells with the same Al mole fraction $x=0.2$. (1) The potential shape at the bottom of each quantum the well has a slight downward bowing for well-doped case (where the electron charge distribution nearly cancels the dopant charge distribution), and has a

large upward bowing for the other case (where the charge distribution of electrons and dopants are spatially separated). (2) For the well-doped case all eight quantum wells have almost the same potential minimum, whereas for the barrier-doped case the potential minimum of the well near the center is much lower than that of the well near the edge. (3) In the barrier-doped case, two additional quantum wells (one on each side) with a parabolic potential are formed at the outermost doped $Al_xGa_{1-x}As$ layers [see Figs. 1(b) and 1(c)]. We shall refer to these quantum wells as the parabolic $Al_xGa_{1-x}As$ wells. All these will affect the energy separations between the lowest-lying subbands, and therefore the peak positions of the intersubband plasmons. Thus, we expect the Raman spectra to be sensitive to the doping profile.

In Fig. 2, we show the calculated Raman spectra of multiple GaAs-$Al_{0.2}Ga_{0.8}As$ quantum wells doped with (a) $n_{2D}=3.0\times10^{12}$ cm^{-2}, (b) $n_{2D}=5.7\times10^{12}$ cm^{-2}, and (c) $n_{2D}=1.06\times10^{13}$ cm^{-2} in each quantum well. The Fermi levels in these structures are 75, 120, and 180 meV, respectively above the lowest confined level. Both the well and barrier widths are kept at 100 Å, and $N_w=8$. In our calculation, $N_c=16$ (since there are two confined levels for each quantum well) and $N=48$. The total potential profile for (c) has been shown in Fig. 1(a). In each plot, the dashed curve is the result with the interaction ($\tilde{V}$) set to zero (noninteracting spectrum) and the solid curve is the full result. In (a), the Fermi level is slightly above the minimum of the second subband, so the lowest confined subband in each quantum well is heavily occupied and the second subband is lightly occupied, while the higher subbands are essentially empty. The transition from the first to the second subband (labeled 1-2) in each quantum well leads to an intersubband transition peak at around 600 cm^{-1} in the noninteracting spectrum (the dashed curve), and its corresponding intersubband plasmon peak is around 850 cm^{-1} when the Coulomb interaction is included (solid curve). Note that the intersubband plasmon mode is a collective mode which is a linear combination of the 1-2 intersubband transition (the predominant component) and many other electronic excitations (some of them correspond to forbidden transitions). In (b), the first subband is more heavily occupied, and the second subband becomes partially occupied. The 1-2 transition is stronger than that in (a) due to the increase in the factor (n_1-n_2), where n_i is the 2D carrier density in subband i [see Eq. (20)], and the Coulomb shift is larger. The peak position of the 1-2 plasmon moves to around 930 cm^{-1}. The larger factor (n_1-n_2) also enhances the effective interaction $\tilde{V}$, thus leading to a larger Coulomb shift. Note that if the temperature considered was zero, and the subbands were parabolic, then the factor (n_1-n_2) would remain constant as long as the Fermi level is above the minimum of the second subband. However, at room temperature, there is substantial ''spillover'' from subband 1 to 2, when the Fermi level is near the minimum of subband 2; thus, the factor (n_1-n_2) increases from (a) to (b). Furthermore, the increase of energy spacing between subbands 1 and 2 as the density increases due to the downward bowing of the quantum-well potential also causes the factor (n_1-n_2) to increase. In (c), the lowest two confined subbands are heavily occupied, and some of the higher unconfined subbands also become lightly occupied. An additional shoulder feature labeled 2-3* becomes apparent in the noninteracting spectrum, where 3* denotes a ''third'' energy level, which corresponding to a resonance in the unconfined continuum states. Once the Coulomb interaction is included, the 1-2 transition is shifted to around 1010 cm^{-1}. The shoulder structure also moves up to around 1100 cm^{-1}. The Coulomb shift for this is smaller, since the factor (n_2-n_3) is smaller than (n_1-n_2). Since many higher levels are occupied, the Raman spectrum contains many intersubband plasmon transitions and it has a much broader feature.

In Fig. 3, we show the calculated Raman spectra of barrier-doped multiple GaAs-$Al_{0.2}Ga_{0.8}As$ quantum wells with (a) $n_{2D}=2.9\times10^{12}$ cm^{-2}, (b) $n_{2D}=5.4\times10^{12}$ cm^{-2}, and (c) $n_{2D}=1.20\times10^{13}$ cm^{-2} per quantum well. Here n_{2D} is the total 2D density of the MQW structure divided by N_w, although there are N_w+1 doped barrier regions. Here $N_c=18$ for (a) and (b), since there are two additional confined states in the parabolic $Al_xGa_{1-x}As$ wells, and $N=48$. For (c), we used $N_c=28$, since more subband states become occupied. The Fermi levels in these structures are 65, 90, and 170 meV, respectively, above the lowest confined level. Both the well and barrier widths are kept at 100 Å. The total potential profile for (c) has been shown in Fig. 1(b). Without interaction, the 1-2 transition peaks at around 500 cm^{-1} for case (a) (lowest density) and shifts to lower energy [at around 400 cm^{-1} for (b) and 200 cm^{-1} for (c)] as the 2D density increases. This is caused by the change in potential profile at the bottom of the quantum well, which goes from a slight upward bowing at low density to a very large upward bowing at high density [see Fig. 1(b)]. The upward bowing tends to reduce the 1-2 energy separation, since the wave function of level 1 is peaked at the center and influenced most by the bowing, while the wave function of level 2 has a node at the center, and hence is much less affected by the bowing. The reduction in 1-2 energy spacing tends to reduce the factor (n_1-n_2), while the increase of the Fermi level tends to increase it. The two competing mechanisms cause (n_1-n_2) to increase slightly from (a) to (b), then decrease from (b) to (c). This factor, however, cannot account for the increase of oscillator strength of the 1-2 peak (see dashed curves) from (b) to (c). It turns out that although (n_1-n_2) is reduced from (b) to (c), the number of subband ''1'' is nearly doubled in case (c), as the large upward bowing essentially divides each quantum well into two triangular wells. This is why we choose $N_c=28$ insted of 18. The strength of the 1-2 transition is greatly enhanced compared with (b). Furthermore, since the Fermi level is so high, many transitions involving highers subbands contribute to the additional structures in the noninteracting spectrum (see shoulder structures of the dashed curve).

When the interaction is included, the 1-2 plasmon mode peaks at higher wave number than the 1-2 transition, just as in the well-doped case. In (b), a shoulder structure due to the 2-3* transition is again present (at around 800 cm^{-1}). Furthermore, a feature labeled 1*-2 is found at energies below 200 cm^{-1}. Here 1* labels the lowest confined level of the parabolic $Al_xGa_{1-x}As$ wells formed at outermost doped $Al_xGa_{1-x}As$ layers, whose energy is about 10–15 meV below the second confined level (level 2) of the neighboring GaAs quantum well. When the Coulomb interaction is included, this transition couples with the 1-2 transition and

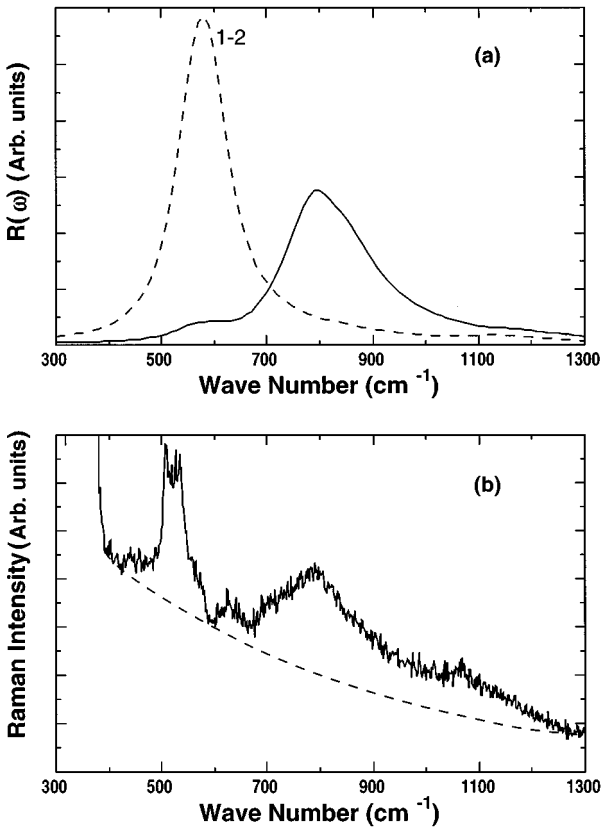

FIG. 5. Raman spectra of well-doped multiple GaAs-$Al_{0.2}Ga_{0.8}As$ quantum wells with $L_w = L_b = 100$ Å and $n_{2D} \approx 3.7 \times 10^{12}$ cm^{-2}. (a) Theory; dashed curves: without Coulomb interaction; solid curves: full calculation. (b) Experiment; the dashed curve indicates the background from the tail of Raman phonon signals.

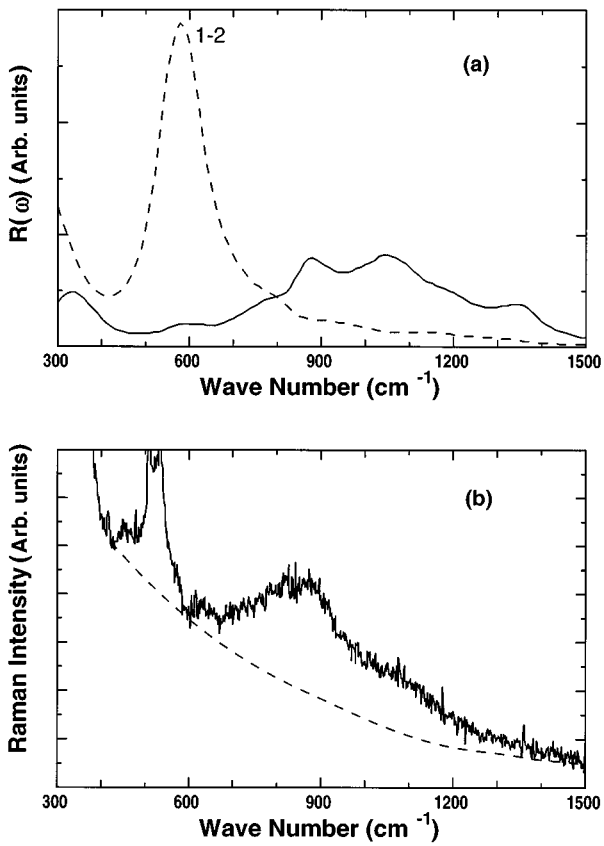

FIG. 6. Raman spectra of well-doped multiple GaAs-$Al_{0.2}Ga_{0.8}As$ quantum wells with $L_w = L_b = 100$ Å and $n_{2D} \approx 9.6 \times 10^{12}$ cm^{-2}. (a) Theory; dashed curves: without Coulomb interaction; solid curves: full calculation. (b) Experiment; the dashed curve indicates the background from the tail of Raman phonon signals.

gives rise to a bump at around 430 cm^{-1}. This feature would not be present if the outermost quantum barriers were not doped. In (c), all 1-2 transitions occur at around 200 cm^{-1}, thus the 1*-2 transition is masked. When the Coulomb interaction is included, the Raman spectrum becomes a broad feature centered at 850 cm^{-1}. Comparing Figs. 2 and 3, we noticed that the Raman spectra are quite different for well-doped and barrier-doped MQW's, even if the electron 2D densities per quantum well are similar, indicating the sensitivity of the Raman spectrum to the doping profile.

In Fig. 4, we show the calculated Raman spectra of barrier-doped multiple GaAs-$Al_{0.4}Ga_{0.6}As$ quantum wells with (a) $n_{2D} = 1.9 \times 10^{12}$ cm^{-2}, (b) $n_{2D} = 4.4 \times 10^{12}$ cm^{-2}, and (c) $n_{2D} = 1.36 \times 10^{13}$ cm^{-2} per quantum well. The Fermi levels in these structures are 64, 105, and 160 meV, respectively above the lowest confined level. Both the well and barrier widths are kept at 100 Å, and $N_w = 8$. The total potential profile for (c) has been shown in Fig. 1(c). Because the quantum well is deeper, we now have three confined levels in each quantum well. Thus we use $N_c = 28$ (four more for confined states in parabolic $Al_xGa_{1-x}As$ wells) and $N = 48$. In (a), the lowest two levels in each quantum well are occupied, thus both 1-2 and 2-3 transitions are present (peaked around 700 and 1020 cm^{-1}) in the noninteracting spectrum. With the interaction turned on they are shifted upwards to 850 and 1050 cm^{-1}, respectively. In (b), the 2-3 transition becomes stronger as the population in the second subband is increased. With the interaction turned on, the second peak gains more strength at the expense of the first peak, and it becomes the dominant peak at around 1100 cm^{-1}. In (c), all three confined levels are occupied, and the transitions from the third confined level to higher subbands (unconfined states) lead to features at energies below 400 cm^{-1}. Also of interest is the structure labeled 1*-2*, which corresponds to the transition from the first subband to the second subband in the parabolic $Al_xGa_{1-x}As$ wells. The energy of level 1* happens to coincides with the energy of level 2 in the GaAs quantum wells, so the 1*-2 transition is absent here. The Coulomb interaction shifts all these peaks upward and modifies their strengths, with higher-energy transitions gaining more strength at the expense of lower-energy transitions.

The comparison between theory and experiment is demonstrated in Figs. 5 and 6. Experimental data are taken for GaAs-$Al_{0.2}Ga_{0.8}As$ multiple quantum wells with $n_W = 8$. The dashed lines in the experimental spectra indicate the background contribution from the tail of Raman phonon signals. The sharp structures between 500 and 550 cm^{-1} are the GaAs second-order phonon signals, which should be omitted

when compared with theoretical calculations presented here. Since the determination of carrier concentration and the doping profile can have uncertainty up to 20%, we can match the data more closely by adjusting the parameters used in our calculation within this uncertainty range. In Fig. 5, the 2D carrier density (determined by the Hall measurements) is around 3.85×10^{12} cm^{-2}, whereas in the theoretical calculation, we have $n_{2D}=3.7\times10^{12}$ cm^{-2}. This is obtained by choosing a Fermi level to be 85 meV above the lowest quantum-well state energy. The theoretical doping profile is described by Eq. (9) with $b=25$ Å. The more defused doping profile used here than that in previous calculations is needed to fit the experimental peak position of the 1-2 intersubband plasmon. Had we used $b=10$ Å, the calculated results would have been similar to that given in Fig. 2(a), and the peak position of the 1-2 intersubband plasmon about 50 cm^{-1} higher. This demonstrates the sensitivity of the intersubband plasmon position to the doping profile. This is because the change in doping profile modifies the net screened potential and therefore the energy separations between quantum-well levels.

In Fig. 6, the experimental 2D density (determined by Hall measurements) is 9.86×10^{12} cm^{-2}, while the theoretical value used is 9.6×10^{12} cm^{-2}. At this high doping level, many higher subbands are partially filled, and the transitions from these subbands to higher subbands give rise to multiple-peak structures in the Raman spectrum. The first structure corresponding to the 1-2 intersubband plasmon is clearly observable (peaked around 880 cm^{-1}), while the second feature centered around 1050 cm^{-1} is barely recognizable from the experimental spectrum. If the background (as indicated by the dashed curve) is subtracted, this feature will become more prominent. We tentatively identify this feature as the 2-3* intersubband plasmon. In the experimental spectrum, the strength of this feature is weaker compared with the 1-2 plasmon mode, while in the theoretical spectrum both the 1-2 and 2-3* plasmon modes have similar peak heights. More theoretical and experimental works are needed to resolve this difference.

IV. SUMMARY

We have presented systematic theoretical studies of the Raman spectra of heavily doped GaAs-Al$_x$Ga$_{1-x}$As multiple quantum wells (MQW's). The band nonparabolicity, the many-body exchange correlation, and the dynamic dielectric screening are all taken into account. We have introduced an ''effective Hamiltonian method'' which maps Dyson's equation for the density-density correlation function into an eigenvalue problem for efficient numerical evaluation of the Raman spectrum. The results are found to be sensitive to the doping profile in the sample, with the prominent intersubband plasmon transition being much lower in energy in the barrier-doped MQW than that in well-doped MQW of the same 2D doping concentration. A close comparison between experimental data and the theoretical simulation can therefore provide information about the actual dopant distribution in these heavily doped MQW's.

ACKNOWLEDGMENTS

This work was supported by the U. S. Army Research Office under Contract No. DAAH04-94-G-0354.

APPENDIX MATRIX ELEMENTS

The matrix elements of $V(q)$ in the basis $\{\phi_n\}$ given by Eq. (6) are defined as

$$\overline{V}_{ij,mn}(q)=\int dz\,dz'\,\frac{2\pi e^2}{q}e^{-q|z-z'|}\times\phi_i(z)\phi_j(z)\phi_m(z')\phi_n(z').$$

Substituting Eq. (6) into the above equation and carrying out the integral, we have

$$\overline{V}_{ij,mn}(q)=\frac{2\pi e^2}{q}[t(i+j,m+n)-t(i+j,m-n)-t(i-j,m+n)+t(i-j,m-n)],$$

where

$$t(m,n)\equiv\frac{1}{L^2}\int_0^L\cos(m\pi z/L)e^{-q|z-z'|}\cos(n\pi z'/L)dz\,dz'$$

$$=\frac{1}{2\pi^2}[1-(-1)^n e^{-qL}][1+(-1)^{m+n}]\left[\frac{mn-p^2}{(p^2-mn)^2+(m+n)^2p^2}-\frac{mn+p^2}{(p^2+mn)^2+(m-n)^2p^2}\right]+\frac{1}{(m^2+p^2)\pi^2}(\delta_{m,n}+\delta_{m,-n})+\frac{2}{qL}\delta_{m,0}\delta_{n,0}$$

and $p \equiv qL/\pi$.

The matrix elements of $V(q)$ between the eigenstates of the MQW system are given by

$$V_{ij,kl}(q) = \sum_{mn,rs} C_m^i C_n^j C_r^k C_s^l \overline{V}_{mn,rs}(q).$$

We define

$$\overline{p}_{mn}(q) = \int_0^L dz e^{iqz} \phi_m(z) \phi_n(z).$$

Substituting (1) into the above, and integrating over z, yields

$$\overline{p}_{mn}(q) = s(m+n) - s(n-m) - s(m-n) + s(-m-n),$$

where

$$s(n) \equiv \frac{1}{2L} \int_0^L dz e^{i(q_z + n\pi/L)z} = -\frac{i[(-1)^n e^{iq_z L} - 1]}{2(q_z L + n\pi)}.$$

The matrix elements $p_{ij}(q_z)$ are given by

$$p_{ij}(q_z) = \sum_{mn} C_m^i C_n^j \overline{p}_{mn}(q_z).$$

[1] A. Pinczuk, J. M. Worlock, H. L. Stömer, R. Dingle, W. Wiegmann, and A. C. Gossard, Solid State Commun. **36**, 43 (1980).
[2] G. Fasol, N. Mestres, H. P. Hughes, A. Fisher, and K. Ploog, Phys. Rev. Lett. **56**, 2517 (1986).
[3] C. Schüller, J. Kraus, and G. Schaack, Phys. Rev. B **50**, 18 387 (1994).
[4] M. H. Degani, J. Appl. Phys. **70**, 4362 (1991).
[5] H. C. Casey, Jr. and M. B. Panish, *Heterostructure Lasers* (Academic, New York, 1978), Part A.
[6] W. T. Tsang, E. F. Schubert, and J. E. Cunningham, Appl. Phys. Lett. **60**, 116 (1992).
[7] L. A. O. Nunes, Phys. Rev. B **47**, 13 011 (1993).
[8] L. Wendler and E. Kändler, Phys. Status Solidi B **177**, 9 (1993).
[9] H. Yao and A. Compaan, Appl. Phys. Lett. **57**, 9 (1990).
[10] J. Kraus and D. Hommel, Semicond. Sci. Technol. **10**, 785 (1995).
[11] J. K. Jain and P. B. Allen, Phys. Rev. B **32**, 997 (1985).
[12] J. K. Jain and S. Das Sarma, Phys. Rev. B **36**, 5949 (1987).
[13] H. Yao, M. Mohiuddin, Y.C. Chang, E.F. Schubert, and L. Pfeiffer (unpublished).
[14] G. Bastard, Phys. Rev. B **25**, 7584 (1982).
[15] G. Lindemann, R. Lassning, W. Seidenbusch, and E. Gornik, Phys. Rev. B **28**, 6157 (1983).
[16] H. Casey Jr., A. Y. Cho, D. V. Lang, and E. H. Nicollian, J. Vac. Sci. Technol. **15**, 1408 (1976).
[17] D. J. Wolford, T. F. Keuch, J. A. Bradley, M. A. Gell, D. Ninno, and M. Jaros, J. Vac. Sci. Technol. B **4**, 1043 (1986).
[18] S. Adachi, J. Appl. Phys. **58**, R1 (1985).
[19] W. Kohn and L.J. Sham, Phys. Rev. **140A**, 1133 (1965).
[20] D. M. Ceperley and B. J. Alder, Phys. Rev. Lett. **45**, 566 (1980).
[21] J. Perdew and A. Zunger, Phys. Rev. B **23**, 5048 (1981).